
ARCHIVIO ISTITUZIONALE DELLA RICERCA

Updated Europa gravity field and interior structure from a reanalysis of Galileo tracking data / Gomez Casajus L.; Zannoni M.; Modenini D.; Tortora P.; Nimmo F.; Van Hoolst T.; Buccino D.; Oudrhiri K.. - In: ICARUS. - ISSN 0019-1035. - STAMPA. - 358:(2021), pp. 114187.1-114187.7. [10.1016/j.icarus.2020.114187]

Alma Mater Studiorum Università di Bologna
Archivio istituzionale della ricerca

Updated Europa gravity field and interior structure from a reanalysis of Galileo tracking data

This is the final peer-reviewed author's accepted manuscript (postprint) of the following publication:

Published Version:

Availability:
This version is available at: https://hdl.handle.net/11585/796411 since: 2022-10-13

Published:

DOI: http://doi.org/10.1016/j.icarus.2020.114187

Terms of use:

Some rights reserved. The terms and conditions for the reuse of this version of the manuscript are specified in the publishing policy. For all terms of use and more information see the publisher's website.

This item was downloaded from IRIS Università di Bologna (https://cris.unibo.it/).
When citing, please refer to the published version.

(Article begins on next page)

06 May 2024

This is the final peer-reviewed accepted manuscript of:

Gomez Casajus, L., Zannoni, M., Modenini, D., Tortora, P., Nimmo, F., Van Hoolst, T., Buccino, D.R., Oudrhiri, K., 2021. Updated Europa gravity field and interior structure from a reanalysis of Galileo tracking data. Icarus 358, 114187.

The final published version is available online at:

https://doi.org/https://doi.org/10.1016/j.icarus.2020.114187

Rights / License:

The terms and conditions for the reuse of this version of the manuscript are specified in the publishing policy. For all terms of use and more information see the publisher's website.

This item was downloaded from IRIS Università di Bologna (https://cris.unibo.it/)

When citing, please refer to the published version.

Updated Europa Gravity Field and Interior Structure from a Reanalysis of Galileo Tracking Data

Luis Gomez Casajus[1,2*], Marco Zannoni[1,2], Dario Modenini[1], Paolo Tortora[1,2], Francis Nimmo[3], Tim Van Hoolst[4,5] Dustin Buccino[6], Kamal Oudrhiri[6]

[1]Dipartimento di Ingegneria Industriale, Università di Bologna, Forlì, Italy

[2]Centro Interdipartimentale di Ricerca Industriale, Università di Bologna, Forlì, Italy

[3]Department of Earth & Planetary Sciences, University of California Santa Cruz, Santa Cruz, California, USA

[4]Royal Observatory of Belgium, Ringlaan 3, 1180 Brussels, Belgium

[5]Institute of Astronomy, KU Leuven, Celestijnenlaan 200D, 3001 Leuven, Belgium

[6]Jet Propulsion Laboratory, California Institute of Technology, Pasadena, California, USA

[*]Corresponding author.

Abstract

The Galileo radio tracking data were reanalysed exploiting the new knowledge of Jupiter obtained by the Juno mission, together with modern orbit determination techniques developed for the Cassini data analysis. Using Doppler data acquired during six encounters of Europa an updated gravity field of the moon was obtained, resulting in a value of C_{22} statistically different from the available literature. The new value suggests a thinner ice-water shell and a less dense interior.

Keywords: *Europa, Interiors, Orbit determination, Jupiter, satellites, Geophysics*

1. Introduction

The Galileo mission studied the Jovian system for eight years, from December 1995 to September 2003. One of the main mission objectives was the study of Europa, the smallest of the Jovian moons discovered by Galileo Galilei in 1610, and the sixth biggest moon of the entire solar system. Before the arrival of the Galileo spacecraft to the Jovian system, very little was known about Europa. The mission provided plenty of data

© 2021. Licensed under the Creative Commons CC-BY-NC-ND 4.0
http://creativecommons.org/licenses/by-nc-nd/4.0/

which dramatically increased our knowledge of the moon and resulted in the discovery of a subsurface ocean of liquid water (Carr et al., 1998; Kivelson et al., 2000; Zimmer et al., 2000), with important implications for its habitability.

The gravity field of a celestial body is crucial to understand its interior structure and composition. Using Galileo data, three different analyses of Europa's gravity field were performed. The first gravity field analysis, (Anderson et al., 1997), analysed independently the non-coherent radiometric data acquired during E4 (December 1996) and E6 (February 1997), according to the numbering scheme used by the Galileo project, providing a weighted mean of the single orbital fits in which the hydrostatic equilibrium constraint (J_2/C_{22} = 10/3 for a relaxed, synchronously rotating, satellite) was applied. From the Radau relation the moment of inertia (MoI) factor was retrieved directly from the degree-2 gravity field coefficients, obtaining a MoI = 0.330 ± 0.014. This analysis concluded that the measurements were compatible with a metallic core surrounded by a water ice-liquid outer shell. Subsequently (Anderson et al., 1998), performed a global fit using four Europa flybys, adding E11 (November 1997) and E12 (December 1997) to the previous solution, along with ground-based astrometric data and optical navigation observables from both Voyager and Galileo, applying the hydrostatic equilibrium as an a priori constraint. The analysis provided evidence that the Galilean moon is most likely differentiated into a metallic core surrounded by a rock mantle and a water outer shell in liquid or solid state. Finally, (Jacobson et al., 1999) reported on the reconstruction of Galileo's orbit during the prime mission and the estimation of Jupiter's satellite ephemerides by means of a global fit. The analysis used an extensive data set comprising Earth-based astrometry, Pioneer and Voyager radiometric and optical data, and Galileo radiometric data up to E19 (February 1999), also introducing the a priori equilibrium constraint between J_2 and C_{22}. The estimated J_2 and C_{22} coefficients were substantially smaller than those published in the last reference work (Anderson et al., 1998).

The entire Galileo mission included 11 encounters of Europa, 8 of which were close enough to provide information about its mass and gravity field. In this work, only the best 6 encounters, in terms of data quality and availability, are used. The main characteristics of Galileo's flybys of Europa are summarized in Table 1,

© 2021. Licensed under the Creative Commons CC-BY-NC-ND 4.0
http://creativecommons.org/licenses/by-nc-nd/4.0/

while Figure 1 shows the corresponding ground tracks. Unfortunately, all the encounters were nearly equatorial, so we do not expect a good accuracy in the determination of the J_2 gravity coefficient (which is longitudinally symmetric). As can be seen in Table 1, the orbital distribution of the flybys in terms of mean anomaly of Europa around Jupiter, together with the non-negligible eccentricity of the Galilean satellite, suggest that in principle the tidal response to Jupiter could be inferred.

In this paper we present the reanalysis of Galileo tracking data acquired during the different encounters with the Galilean moon motivated by the future ESA's JUICE (Grasset et al., 2013) and NASA's Europa Clipper (Phillips et al., 2014) missions, which will study Ganymede, Europa, and Callisto, and by recent advancements in the knowledge of the Jupiter system.

First, NASA's Juno mission recently provided a new estimation of the gravity field of Jupiter, which drives the orbital motion of the moons, to an unprecedented level of accuracy (Folkner et al., 2017; Iess et al., 2018; Serra et al., 2019, Durante et al., 2020). The zonal harmonic coefficients up to degree 10 were determined up to 50 times more accurately than before and, for the first time, non-zero values for the odd zonal harmonic coefficients up to degree 9 were observed and related to Jupiter's wind dynamics (Kaspi et al., 2018, Guillot et al., 2018).

In addition, Juno provided new observations of the Io Plasma Torus (IPT), a toroidal cloud of plasma that orbits Jupiter (Iess et al., 2018), from which new models were derived (Phipps et al., 2018). The IPT introduces a non-dynamical, dispersive signal on the radiometric observables and becomes a source of bias in the gravity estimations, if not properly accounted for. The effect on the gravity analysis of the Galileo mission is critical, since the probe had to use the S-band, more affected by this dispersive phenomenon than higher frequency radio links currently used.

During the last years, several authors reported evidence of water plumes emerging from Europa (Roth et al., 2014; Sparks et al., 2016). More recently, (Jia et al., 2018) performed a reanalysis of Galileo magnetometer data acquired during E12, suggesting the presence of a plume, localized around 245° W and 5° S, in a region

© 2021. Licensed under the Creative Commons CC-BY-NC-ND 4.0
http://creativecommons.org/licenses/by-nc-nd/4.0/

with high surface temperature (Spencer et al., 1999). This plume may have influenced the motion of the Galileo spacecraft during the encounter, potentially biasing the gravity field analysis.

Moreover, the current analysis is performed using new orbit determination codes and techniques extensively used for the Cassini radio science experiment, in order to provide an update on the gravity field of the moon and report on its internal structure implications.

This manuscript is organised as follows: Section 2 describes the data analysis; Section 3 provides the gravity field results; Section 4 details the implications on the interior structure of Europa; finally, Section 5 summarizes the main conclusions of this work.

2. Data Analysis

The gravity field of Europa can be estimated through reconstruction of Galileo's trajectory during encounters with the moon, exploiting the Doppler shift of a highly stable microwave signal induced by the relative motion between the tracking stations of the Deep Space Network (DSN) and the Galileo spacecraft.

During the different flybys of the Galileo probe with Europa, Doppler data at S-Band (2.3Ghz) were acquired by the 70-m antennas at the DSN complexes of Goldstone, Madrid and Canberra. The Galileo spacecraft operated using only the low-gain antenna at S-band, because Galileo's umbrella-like High Gain Antenna (HGA), which supported X-band, failed to correctly deploy. Therefore, the spacecraft downlink data rate was significantly reduced, limiting the mission science return, and the spacecraft tracking was carried out using the S-band link, which has larger noise and thus lower performances (Iess et al., 2012).

From all the available data (E4, E6, E11, E12, E14, E16, E19, and E26) we only used the 6 flybys that had accessible both tropospheric and ionospheric calibrations, leaving E4 and E26 out of the analysis. The actual length of each arc is determined by the available data in the vicinity of each encounter (Table 1).

© 2021. Licensed under the Creative Commons CC-BY-NC-ND 4.0
http://creativecommons.org/licenses/by-nc-nd/4.0/

Data selection was performed by preferring two-way data over three-way, if an overlap occurs. During E19 we used also one-way data acquired during the closest approach, due to the large sensitivity to the gravity field and the exceptional observed data quality of the obtained residuals. To account for a possible drift of the on-board clock, we estimated a constant bias and linear drift during the one-way tracking pass. Moreover, an additional solution was generated without using one-way data to assess the stability of the retrieved results, obtaining a compatible solution within 1-σ.

Data acquired with an elevation angle, as viewed from the DSN complex, lower than 15° were discarded to avoid potential biases coming from incorrect troposphere or ionosphere calibrations.

The HGA failure prevented the use of multi-frequency link calibration systems (Bertotti et al., 1993; Mariotti et al., 2013), which could have been used to remove the systematic signal due to dispersive media. Since S-band data are significantly affected by dispersive noise, we studied in detail two sources of dispersive noise, the ionosphere of Europa and the IPT, that potentially could have introduced a bias in the gravity results. To do so, we generated the expected Doppler shift induced by these dispersive sources using reference models (Kliore et al., 1997; Phipps et al., 2018), finding that the ionosphere could have corrupted the one-way data acquired during the closest approaches of E4, E6, and E26, and that the IPT could explain some strong signatures found in the two-way tracking data of E26. Since the models cannot be used to calibrate the observables at the required level of accuracy, we decided to remove from the analysis about 12 minutes of possibly corrupted, non coherent, data of E6, whereas E4 and E26 were not used at all, to prevent errors in the gravity solution.

	Date of C/A	Altitude (km)	Rel. Velocity (km/s)	Inclin. (°)	Mean anomaly (°)	SEP (°)	Number of points	RMS at 60 s (mm/s)
E4	19 Dec. 1996	693.0	5.75	178	-137	25	N/A	N/A
E6	20 Feb. 1997	587.0	5.77	162	-142	25	2189	0.869

© 2021. Licensed under the Creative Commons CC-BY-NC-ND 4.0
http://creativecommons.org/licenses/by-nc-nd/4.0/

E11	06 Nov. 1997	2044.6	5.72	26	41	89	1324	0.317
E12	16 Dec. 1997	201.9	6.27	9	127	55	1309	0.509
E14	29 Mar. 1998	1644.9	6.42	12	-149	26	1506	0.871
E16	21 Jul. 1998	1835.2	6.22	26	-63	120	1285	0.165
E19	1 Feb. 1999	1440.5	5.83	149	36	46	994	0.334
E26	3 Jan. 2000	351.3	11.3	133	-143	103	N/A	N/A

***Table 1**: Main characteristics of the different Galileo encounters of Europa. The table reports on the date of the closest approach (C/A), the minimum altitude, the relative velocity of the spacecraft, the orbital inclination, the mean anomaly in Europa's orbital frame, the Sun-Earth-Probe (SEP) angle, the number of Doppler points used, and the Root Mean Square (RMS) of the Doppler residuals at 60 s. Note that E4 and E26 data were not used in the analysis.*

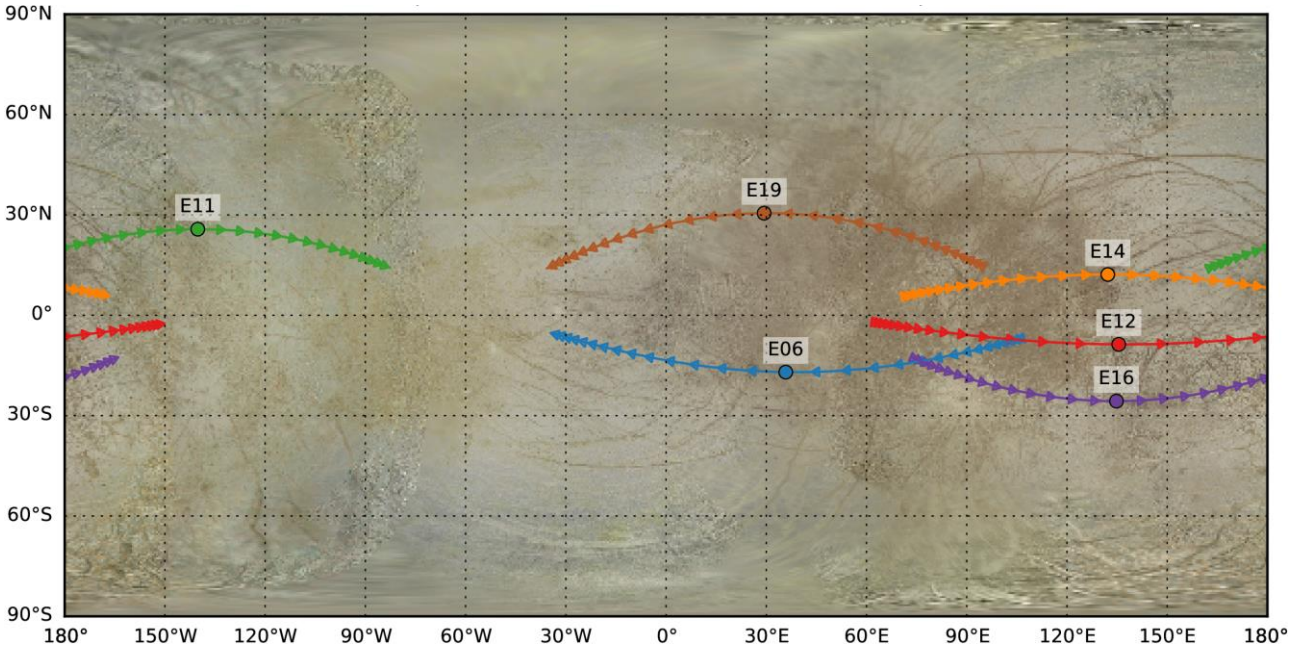

***Figure 1**: Ground tracks of Galileo during the different Europa encounters 15 minutes before and after the C/A. The C/A is indicated by a circle and the separation between the different markers is equal to 60 s. The equatorial region of the moon is well sampled, while the higher latitudes are not covered. The ground tracks are represented over a map of Europa produced by Björn Jónsson (Planetary Society) using Galileo and Voyager images (NASA, JPL).*

© 2021. Licensed under the Creative Commons CC-BY-NC-ND 4.0
http://creativecommons.org/licenses/by-nc-nd/4.0/

129 The range-rate data were compressed at 60 second integration time, as a balance between spatial resolution
130 and numerical considerations (Zannoni and Tortora, 2013), and were weighted on a pass-by-pass basis, using
131 the root mean square of their residuals. The data were analysed with JPL's orbit determination code MONTE
132 (Evans et al., 2018), which adopts a Batch-Weighted Least Squares information filter (Bierman 1977), that
133 allows to generate iterative corrections to an a-priori dynamical model.

134 The dynamical model included the gravitational acceleration due to the Sun and the planets of the Solar
135 system, including Jupiter and its Galilean satellites. For Jupiter, we used the latest gravity solution obtained
136 by the Juno gravity team up to the 10th degree (Iess et al., 2018), while for the other Galilean satellites we
137 used the 2nd degree and order gravity fields reported by the Radio Science Team and summarized in
138 (Schubert et al., 2004). For Europa, we adopted a perfectly-synchronous rotational model, in which the
139 moon's long axis points to the empty focus of the orbit, and set the obliquity equal to zero. The diurnal
140 libration on Europa is expected to be ~150 m (Van Hoolst et al. 2013), or 0.005°, and the librations related to
141 deviations from a Keplerian orbit can be of the order of 0.05° (Rambaux et al. 2011). The obliquity is predicted
142 to be 0.05° (Baland et al. 2012, Chen et al. 2014). These angles are much smaller than the retrieved
143 uncertainty on the misalignements between the body-fixed frame and the inertia axes and neglecting them
144 does not affect our conclusions in a detectable way. For Jupiter we used the rotational model used to
145 generate the JUP310 ephemerides (The satellite ephemerides of Jupiter can be retrieved from
146 ftp://ssd.jpl.nasa.gov/pub/eph/). We included the non-gravitational acceleration due to Solar Radiation
147 Pressure (SRP) acting on the spacecraft, estimated to be around 3.3 nm/s^2 during the Jupiter approach phase
148 (Antreasian et al., 1997). In addition, as a stability test, we introduced the possible drag produced by a plume
149 during E12 (discussed in Section 3), and the non-isotropic acceleration of the Radioisotope Thermal
150 Generators (RTG's), modelled using an exponential acceleration.

151 To analyse the data, we adopted a multi-arc approach (Milani et al., 2010), a well-known technique used in
152 the analyses of radio science data of several deep space missions (Iess et al., 2012; Iess et al., 2014; Modenini
153 & Tortora, 2014; Tortora et al., 2016; Iess et al., 2019; Durante et al., 2019; Zannoni et al., 2018, Zannoni et

© 2021. Licensed under the Creative Commons CC-BY-NC-ND 4.0
http://creativecommons.org/licenses/by-nc-nd/4.0/

al., 2020, Lainey et al., 2020), in which radiometric data obtained during non-contiguous orbital segments, called arcs, are jointly analysed to produce a single solution of a set of global parameters, which affect all the arcs, and a set of local parameters that influence only one single arc.

In some of these previous analyses, the orbit of the moon under study was integrated for the entire time span of the data, in order to ensure the coherency of the observed data with the satellite trajectory. However, Durante et al. (2019), highlighted that this kind of analysis is sensitive to errors, mis-modelling or missing models in the ephemeris integration. Since the generation of a coherent Europa ephemeris set was beyond the scope of this work, the state of Europa was treated as a local parameter, updating the orbit of the moon for each encounter, as done in (Durante et al., 2019; Zannoni et al., 2020). This introduces an over-parametrization that can absorb the modelling errors of the ephemerides, avoiding biases in the gravity field.

Our global parameters included Europa's mass and the full gravity field of degree 2, while our local parameters included the initial state vectors of Galileo and Europa. The a priori values of Galileo's state vectors were taken from the last reconstruction of the Galileo navigation team (Retrieved from https://naif.jpl.nasa.gov/pub/naif/GLL/kernels/spk/) with an a priori uncertainty large enough to not constrain the solution. The a priori values of Europa's state vector were retrieved from the latest available Jupiter system ephemerides (JUP310), using a conservative approach for the a priori uncertainty. In addition, we estimated a scale factor for the SRP acceleration for each arc, Doppler biases for three-way data (caused by asynchronous clocks at the transmitting and receiving stations), and a Doppler bias and a drift for the one-way pass of E19. There were not enough data to estimate the rotational parameters of Europa, thus the rotational model is supposed perfectly known.

3. Gravity field results

The estimated set of parameters was sufficient to fit the data to the noise level (Figure 2). Table 2 reports the estimated gravity field coefficients of Europa for two interesting cases. SOL-A represents the unconstrained solution, obtained without imposing the hydrostatic equilibrium ratio J_2/C_{22} = 10/3. The

© 2021. Licensed under the Creative Commons CC-BY-NC-ND 4.0
http://creativecommons.org/licenses/by-nc-nd/4.0/

179 solution is compatible with a body in hydrostatic equilibrium within 1-σ, but the uncertainty in J_2 is very large,
180 due to the poor latitudinal coverage of the flybys. Hence, solution SOL-B was generated applying the
181 hydrostatic equilibrium constraint. We note that this is an assumption, which may or may not turn out to be
182 correct; the main reason for doing so is to allow comparison with previous works, all of which made the same
183 assumption.

184 For the same reason, we imposed the hydrostatic equilibrium constraint equal to the classical value of 10/3,
185 as in the previous solutions available in literature. However, using the more correct value of 3.324, adopted
186 in Section 4, which takes into account the relatively rapid rotation of Europa (Tricarico 2014), the estimated
187 quadrupole coefficients change by less than 0.02-σ.

© 2021. Licensed under the Creative Commons CC-BY-NC-ND 4.0
http://creativecommons.org/licenses/by-nc-nd/4.0/

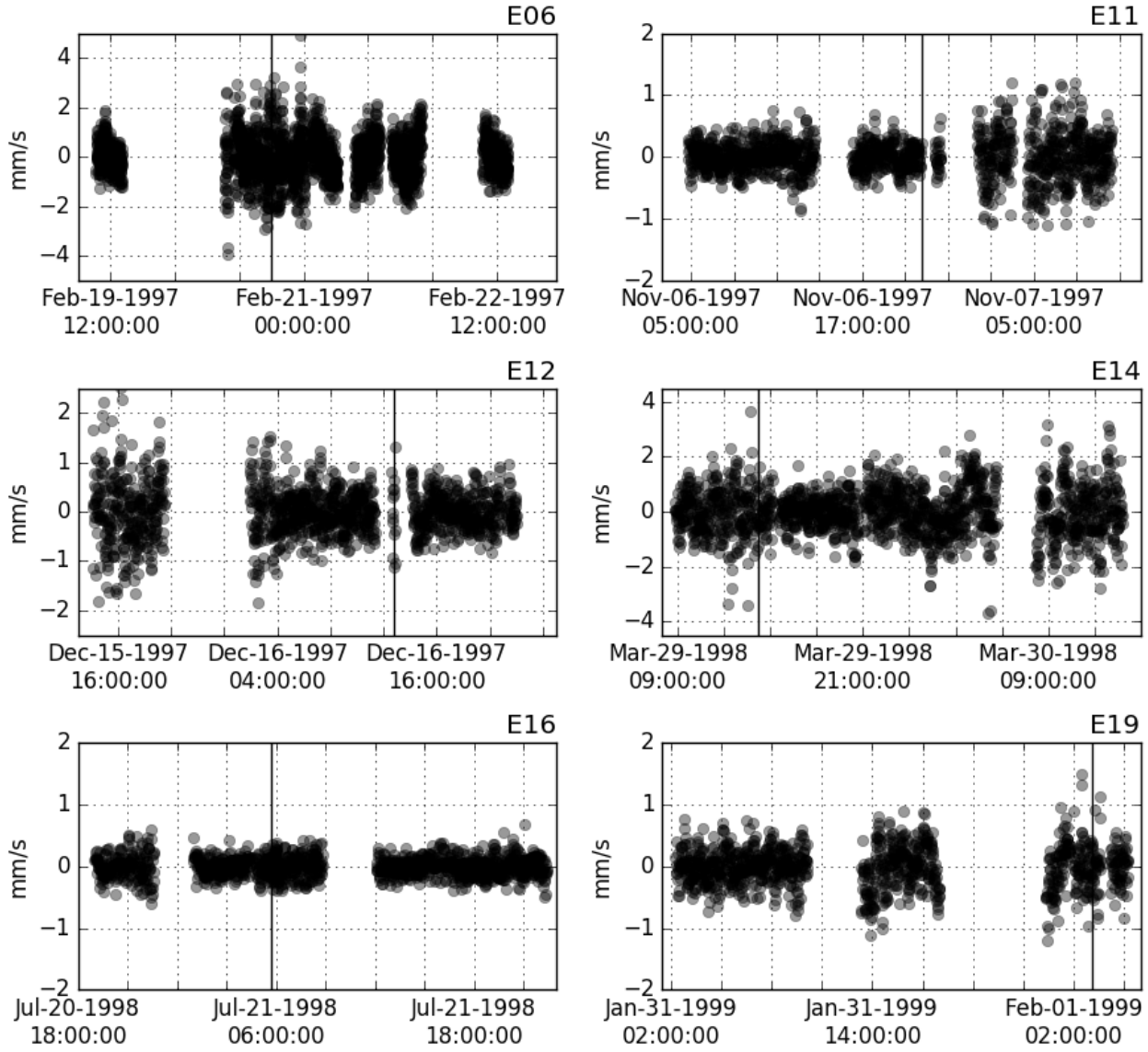

***Figure 2**: Range-rate residuals around the closest approach of E06, E11, E12, E14, E16 and E19 encounters (vertical line), in mm/s. Range-rate residuals are obtained scaling the Doppler residuals by the coefficient 136.27 mm/s x 1/Hz.*

As shown in Figure 3, both solutions are compatible within 1-σ, but SOL-B has smaller uncertainties (as expected, due to the hydrostatic constraint), up to about 1 order of magnitude for J_2 and by 3.7 % for C_{22}.

Given the estimated values of C_{21}, S_{21} and S_{22} and following MacCullagh's theorem we can extract the misalignment between the Europa body fixed frame and its principal axes of inertia. The obtained values

© 2021. Licensed under the Creative Commons CC-BY-NC-ND 4.0
http://creativecommons.org/licenses/by-nc-nd/4.0/

correspond to rotations of -3.1 ± 5.0° and 0.1 ± 1.2° around the x and y axes, respectively. Both are compatible with zero within 1-σ. On the other hand, S_{22} translates to a misalignment of the minimum inertia axis with respect to prime meridian of 1.3 ± 0.6°, that vanishes within 2.1-σ.

Coefficient (x 10^6)	(Anderson et al., 1998; Schubert et al ., 2004)	(Jacobson et al., 1999)	SOL-A (Unconstrained)	SOL-B (Hydrostatic eq.)
J_2	435.50 ± 8.2	417.0 ± .6.0	437.59 ± 77.47	461.39 ± 7.84
C_{21}	-1.4 ± 6.0	-1.3 ± 3.8	1.26 ± 15.21	4.25 ± 11.73
S_{21}	14 ± 12	11.0 ± 10.0	9.01 ± 11.38	7.425 ± 10.16
C_{22}	131.5 ± 2.5	125.0 ± 2.0	138.62 ± 2.44	138.42 ± 2.35
S_{22}	-11.9 ± 2.9	-10.0 ± 2.0	-6.21 ± 2.90	-6.65 ± 2.51
J_2/C_{22}	3.3118 ± 0.0097	10/3	3.16 ± 0.57	10/3
μ	0.993	1.0	-0.17	1.0

***Table 2**: Europa's unnormalized gravity field coefficients and its associated 1-σ uncertainty, corresponding to a reference radius of 1565 km, estimated using two different approaches. SOL-A corresponds to the unconstrained solution, while in SOL-B the hydrostatic equilibrium constraint was applied. In addition, the table shows both previous reference solutions, the J_2/C_{22} ratio and the correlation (μ) between both J_2 and C_{22} coefficients.*

The retrieved uncertainties in all the coefficients, except J_2 for SOL-A, are comparable to the ones obtained in the old solutions (Anderson et al., 1998; Jacobson et al., 1999). The difference in the J_2 uncertainty in SOL-A comes from the fact that the hydrostatic equilibrium constraint was not applied. This large uncertainty was expected since the encounters were nearly equatorial (see Figure 1).

The analysis provides a C_{22} coefficient significantly larger than the one retrieved in the old solutions and shown in Figure 3. The differences are 2.84-σ with respect to (Anderson et al., 1998) and 5.58-σ with respect

© 2021. Licensed under the Creative Commons CC-BY-NC-ND 4.0
http://creativecommons.org/licenses/by-nc-nd/4.0/

to (Jacobson et al., 1999). These differences may come from the use of a different data pre-processing and data-selection and the different orbit determination techniques used in this work, such as the use of MONTE or the local ephemeris update. For example, a detailed inspection of the residuals published in (Jacobson et al., 1999) showed that previous analyses used all the available data without removing the measurements at low elevation angles. Following the same approach, we obtained a value of C_{22} compatible with (Anderson et al., 1998) within 0.8-σ. This is an indication that the previous published solutions might be biased due to the wrong calibration of the Earth's atmosphere and ionosphere at low elevation angles.

Among the Galilean satellites, Europa has the highest eccentricity. This fact together with the good coverage of Galileo's flybys along Europa's orbital frame supported the addition of the tidal parameter k_2 to the estimated parameters set. We found $k_2 = 0.29 \pm 0.46$ (SOL-A) and $k_2 = 0.15 \pm 0.28$ (SOL-B), 1-σ uncertainties. In both cases the retrieved uncertainty is too large to extract any conclusions and only provides upper limits to Europa's tidal response.

A full degree 2 gravity field was sufficient to fit the data. Higher degrees cannot be determined with enough accuracy, but the addition of the full degree 3 and 4 coefficients to the estimated parameters did not bias the solution. The a priori uncertainties of the degree 3 and 4 normalized coefficients were set using the Kaula's rule, K/l^2 (Kaula, 1963), that describes the gravity power spectra of terrestrial planets. The K factor, obtained fitting Titan's gravity field (Durante et al., 2019), was scaled to Europa using the scaling law provided by (Bills et al., 2014), retrieving $K = 2 \cdot 10^{-5}$. Since there is no evidence that the Kaula's rule can be applied to ocean worlds, to assess the stability of the solution we generated other solutions setting the a priori uncertainty of the degree 3 and 4 using 0.1·K and 10·K. The obtained solutions were always compatible within 1-σ.

The possible plume emerging from Europa during the E12 encounter, reported in (Jia et al., 2018), could have perturbed the motion of the Galileo probe, inducing a bias in the solution. For this reason, following a similar approach used for Cassini's flybys close to Enceladus's plumes (Iess et al., 2014), we modelled the perturbation of a plume as an impulsive change in velocity of the spacecraft at the C/A, estimating the three

© 2021. Licensed under the Creative Commons CC-BY-NC-ND 4.0
http://creativecommons.org/licenses/by-nc-nd/4.0/

236 components of this impulse, using an a priori uncertainty of 5 mm/s. The retrieved component along Galileo's
237 velocity is ΔVplume =0.22±4.93 mm/s (SOL-A) and ΔVplume = 0.19±4.93 mm/s (SOL-B), showing that the
238 plume cannot be estimated using the radio tracking data and that therefore it does not represent a bias in
239 the solution.

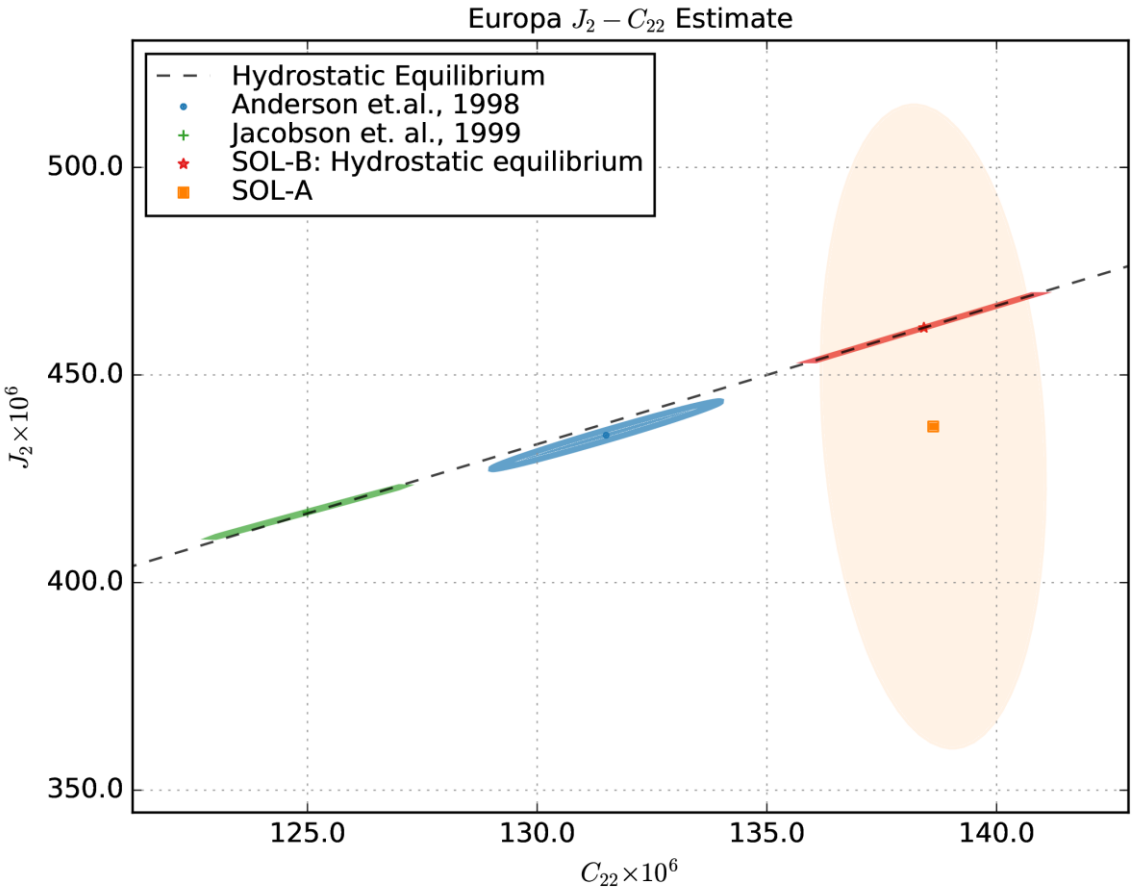

240

241 ***Figure 3:*** *Obtained J_2 and C_{22} and its 1-σ associated error ellipses of SOL-A (unconstrained) and SOL-B (applying the*
242 *hydrostatic equilibrium). In addition, the figure shows both the solutions of (Anderson et al., 1998) and (Jacobson*
243 *et al., 1999), for comparison purposes. The previous published solutions are not compatible with the gravity update*
244 *within 1-σ.*

245 ## 4. Interpretation
246

© 2021. Licensed under the Creative Commons CC-BY-NC-ND 4.0
http://creativecommons.org/licenses/by-nc-nd/4.0/

Given a measurement of either J_2 or C_{22} and assuming hydrostatic equilibrium, the gravity coefficients can then be used to directly infer the MoI of the body (e.g. Schubert et al., 2004). Below we will compare the MoI results obtained from the three different gravity measurements of C_{22} using the hydrostatic assumption. First we will briefly digress to discuss the assumption itself.

If Europa is hydrostatic, then C_{22} can be converted directly to a MoI via the Radau equation (e.g. Schubert et al. 2004). However, we do not *know* that Europa is hydrostatic, because we do not have an independent measurement of J_2. Without further observations, it is unclear whether Europa is likely to be hydrostatic or not. However, the icy moon Titan provides a useful example. Titan's gravity is well-determined (Iess et al. 2010) and the deviation of the ratio J_2/C_{22} is only 2-4% away from the expected hydrostatic ratio. Europa is likely to be more hydostatic than Titan, being more strongly tidally-heated and having a thinner ice shell. We thus regard the hydrostatic assumption as reasonable, though we caution the reader that future gravity measurements may prove it to be incorrect.

Table 3 presents the inferred MoI derived from the three independent solutions. Here we have taken into account the small correction required by Europa's relatively rapid rotation (Tricarico, 2014), the result of which is to modify the ratio J_2/C_{22} from 10/3 to 3.324. The effect of the slightly larger C_{22} coefficient we estimate is to yield a slightly higher MoI, indicating a less differentiated Europa.

Quantity	(Anderson et al., 1998; Schubert et al ., 2004)	(Jacobson et al., 1999)	This Work
C_{22} (x10^6)	131.5 ± 2.5	125.0 ± 2.0	138.42 ± 2.35
MoI	0.3475 ± 0.0026	0.3405 ± 0.0022	0.3547 ± 0.0024
H_2O thickness (1 g/cm^3) (km)	161.8 ± 8.4	184.5 ± 7.2	138.7 ± 7.7
H_2O thickness (0.95 g/cm^3) (km)	157.7 ± 8.2	179.7 ± 7.0	135.2 ± 7.5
Core density (g/cm^3)	3.790 ± 0.049	3.928 ± 0.046	3.658 ± 0.043

© 2021. Licensed under the Creative Commons CC-BY-NC-ND 4.0
http://creativecommons.org/licenses/by-nc-nd/4.0/

H_2O mass fraction (%)	8.6 ± 0.4	9.7 ± 0.4	7.5 ± 0.4

Table 3. *Geophysical parameters derived from C_{22} measurements (see text). Thicknesses and densities are derived assuming a two-layer Europa with a bulk density of 3.013 g/cm^3. The final two rows assume an H_2O density of 0.95 g/cm^3.*

With the known bulk density of Europa (3.013 g/cm^3) and a measurement of its MoI, we can place constraints on its internal structure (e.g. Schubert et al. 2004). The simplest approach is to assume a two-layer structure, with an H_2O layer (ice or water) above a rock/iron core. For an assumed H_2O density (which should be intermediate between that of water and ice), we can deduce the H_2O layer thickness, which is also tabulated in Table 3. While this is undoubtedly an oversimplified model of the real Europa, the point of these calculations is to illustrate how differences in the measured C_{22} value translate into differences in the structures inferred. The higher MoI results in an H_2O layer that is thinner by ~20-40 km than previous estimates. Figure 4 presents these same results graphically, showing how the measured C_{22} values can be mapped to MoI and H_2O layer thickness values.

The same analysis also yields estimates of the core density and H_2O mass fraction (Table 3). Our density is lower than the previous estimates, suggesting a smaller and/or less dense iron component of the rock/iron core. Similarly, the total H_2O mass fraction is a little lower. Although none of these differences are very large, a thinner H_2O layer, as suggested here, would slightly increase the gravitational effect of the mantle, and could in principle slightly shift the characteristic period of tidally-driven resonant oscillations (Matsuyama et al. 2018). The upper-bound SOL-B solution on k_2 of 0.43 is not diagnostic: estimates of Europa's k_2 are typically 0.26 or less (Moore & Schubert 2000). Such a high value would require an ocean density of at least 1500 kg/m^3, if resonant enhancement of tidal flow in the ocean is neglected (e.g. Matsuyama et al. 2018).

© 2021. Licensed under the Creative Commons CC-BY-NC-ND 4.0
http://creativecommons.org/licenses/by-nc-nd/4.0/

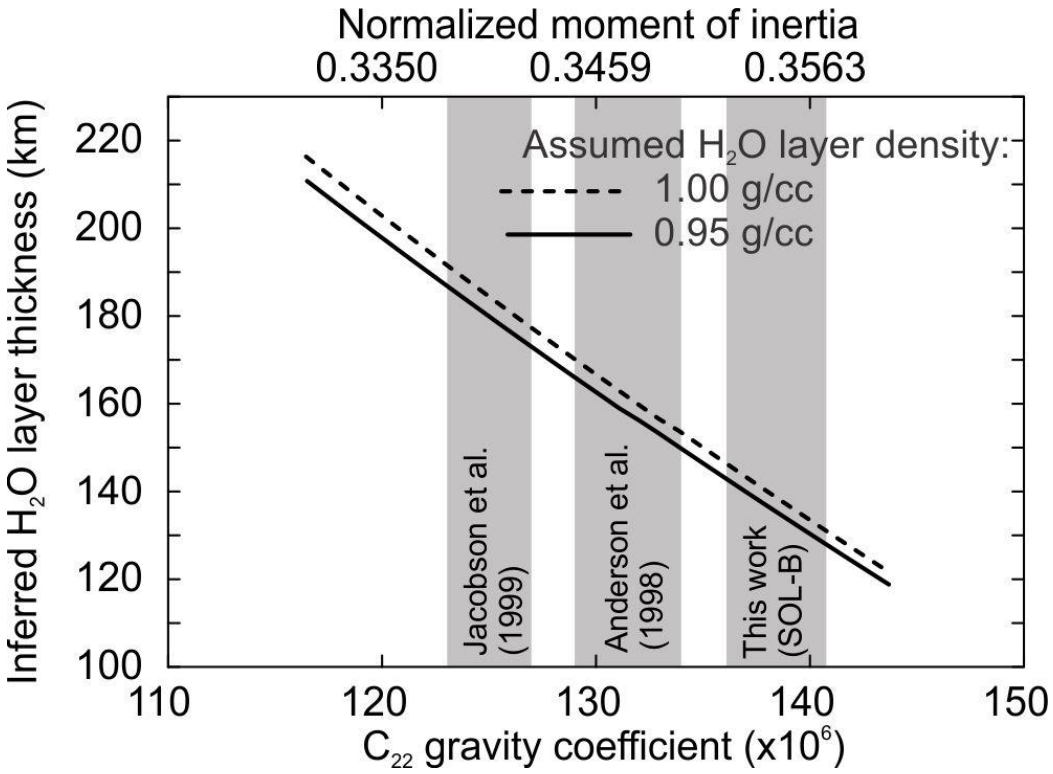

284

285 ***Figure 4.*** *Inferred H_2O layer thickness as a function of C_{22} gravity coefficient (see text), for two different*
286 *assumed H_2O layer densities. Shaded regions denote coefficient estimates made by three different groups.*

287

288 While more complicated (e.g. three-layer) models can be produced (e.g. Schubert et al. 2004), they require
289 additional assumptions to be made. As an example, models which include an iron core or allow an ocean
290 denser than the ice typically result in H_2O thicknesses that are lower than in Table 3 by up to several tens of
291 kilometers. The main point of Table 3 and Figure 4 is to illustrate how different estimates of the gravity
292 coefficients map into different internal structures. The relative differences in, for example, H_2O thickness
293 between the different gravity models will be preserved, even if more complex structures are invoked.

294

295 ## 5. Conclusions
296

© 2021. Licensed under the Creative Commons CC-BY-NC-ND 4.0
http://creativecommons.org/licenses/by-nc-nd/4.0/

In view of the future missions JUICE and Europa Clipper and motivated by the new knowledge of the Jupiter system given by Juno, we reanalysed the radio tracking data of Galileo acquired during the Europa flybys. The analysis considered effects neglected in previous analyses, such as the IPT, Europa's ionosphere, and the recently detected plume of E12, that may have affected the retrieved gravity field. In addition, this work adopted modern orbit determination techniques previously used in the gravity analyses of Cassini and Juno. We obtained a satisfactory fit of the Doppler data, estimating a full degree and order 2 gravity field. The retrieved gravity field is compatible with the hydrostatic equilibrium without imposing the a priori hydrostatic equilibrium constraint (J_2/C_{22} = 10/3), as done in the past in the reference analyses. The obtained C_{22} coefficient is slightly different from previous results and suggests a thinner water ice shell and a less dense core, that could have implications on the characteristic period of tidally-driven resonant oscillations.

Three research groups obtained contrasting solutions of the gravity field of the Galilean satellite using unequal data sets and orbit determination techniques, with slightly different implications on Europa's internal structure. Further insights into Europa's structure and evolution will come from the gravity measurements of the incoming Europa Clipper and JUICE missions. Both of them will allow to estimate the gravity field and the love numbers of the icy moon up to an unprecedented level, shedding light on the interior structure of this body.

6. Acknowledgements

The authors are grateful to William Folkner of Solar System Dynamics Group / JPL for providing the necessary data to carry out this analysis. Thanks to Solar System Dynamics Group and to Robert Haw, former Galileo navigator, for the useful discussions and suggestions regarding the procedures for Galileo data analysis. L.G.C., M.Z., D.M, and P.T. acknowledge Caltech and the Jet Propulsion Laboratory for granting the University of Bologna a license to an executable version of MONTE Project Edition S/W. The work of D.B and K.O was

© 2021. Licensed under the Creative Commons CC-BY-NC-ND 4.0
http://creativecommons.org/licenses/by-nc-nd/4.0/

carried out at the Jet Propulsion Laboratory, California Institute of Technology, under a contract with the National Aeronautics and Space Administration. Government sponsorship acknowledged.

References

Anderson, J. D., Lau, E. L., Sjogren, W. L., Schubert, G., & Moore, W. B. (1997). Europa's differentiated internal structure: Inferences from two Galileo encounters. Science, 276(5316), 1236-1239.

Anderson, J. D., Schubert, G., Jacobson, R. A., Lau, E. L., Moore, W. B., & Sjogren, W. L. (1998). Europa's differentiated internal structure: Inferences from four Galileo encounters. Science, 281(5385), 2019-2022.

Antreasian, P. G., McElrath, T. P., Haw, R.J., & Lewis, J. D. (1998). Galileo Orbit Determination Results During the Satellite Tour, *Advances in the Astronautical Sciences: Astrodynamics 1997*, Vol. 97.

Baland, R.-M., Yseboodt, M., & Van Hoolst, T. (2012). Obliquity of the Galilean satellites: The influence of a global internal liquid layer, Icarus 220, 435-448.

Bertotti, B., Comoretto, G., & Iess, L. (1993). Doppler tracking of spacecraft with multi-frequency links. Astronomy and Astrophysics, 269, 608-616.

Bertotti, B., Iess, L., & Tortora, P. (2003). A test of general relativity using radio links with the Cassini spacecraft. Nature, 425(6956), 374.

Bierman, G. (1977), Factorization Methods for Discrete Sequential Estimation, chap. 8, pp. 162–182, Academic Press, New York.

Bills, B. G., Asmar, S. W., Konopliv, A. S., Park, R. S., & Raymond, C. A. (2014). Harmonic and statistical analyses of the gravity and topography of Vesta. Icarus, 240, 161-173.

Carr, M. H., Belton, M. J., Chapman, C. R., Davies, M. E., Geissler, P., Greenberg, R., ... & Head, J. W. (1998). Evidence for a subsurface ocean on Europa. Nature, 391(6665), 363.

Durante, D., Hemingway, D. J., Racioppa, P., Iess, L., & Stevenson, D. J. (2019). Titan's gravity field and interior structure after Cassini. Icarus.

Durante, D., Parisi, M., Serra, D., Zannoni, M., Notaro, V., Racioppa, P., ... & Folkner, W. M. (2020). Jupiter's gravity field halfway through the Juno mission. Geophysical Research Letters, e2019GL086572.

Evans, S., Taber, W., Drain, T., Smith, J., Wu, H. C., Guevara, M., ... & Evans, J. (2018). MONTE: The next generation of mission design and navigation software. CEAS Space Journal, 10(1), 79-86.

Folkner, W. M., Iess, L., Anderson, J. D., Asmar, S. W., Buccino, D. R., Durante, D., ... & Parisi, M. (2017). Jupiter gravity field estimated from the first two Juno orbits. Geophysical Research Letters, 44(10), 4694-4700.

Grasset, O., Dougherty, M. K., Coustenis, A., Bunce, E. J., Erd, C., Titov, D., ... & Hussmann, H. (2013). JUpiter ICy moons Explorer (JUICE): An ESA mission to orbit Ganymede and to characterise the Jupiter system. Planetary and Space Science, 78, 1-21.

Guillot, T., Miguel, Y., Militzer, B., Hubbard, W. B., Kaspi, Y., Galanti, E., ... & Folkner, W. M. (2018). A suppression of differential rotation in Jupiter's deep interior. Nature, 555(7695), 227.

© 2021. Licensed under the Creative Commons CC-BY-NC-ND 4.0
http://creativecommons.org/licenses/by-nc-nd/4.0/

Iess, L., Budnik, F., Colamarino, C., Corbelli, A., Di Benedetto, M., Fabbri, V., Graziani, A., Hunt, R., James, N., Lanucara, M., Maddè, R., Marabucci, M., Mariotti, G., Mercolino, M., Racioppa, P., Simone, L., Tortora, P., Westcott, M., & Zannoni, M., (2012). ASTRA: Interdisciplinary Study on Enhancement of the End-To-End Accuracy for Spacecraft Tracking Techniques, in: 63rd International Astronautical Congress. pp. 1–11.

Iess, L., Jacobson, R.A., Ducci, M., Stevenson, D.J., Lunine, J.I., Armstrong, J.W., Asmar, S.W., Racioppa, P., Rappaport, N.J., & Tortora, P., (2012). The tides of Titan. Science 337, 457–9. doi:10.1126/science.1219631

Iess, L., Stevenson, D.J., Parisi, M., Hemingway, D.J., Jacobson, R.A., Lunine, J.I., Nimmo, F., Armstrong, J.W., Asmar, S.W., Ducci, M., & Tortora, P., (2014). The gravity field and interior structure of Enceladus. Science 344, 78–80. doi:10.1126/science.1250551

Iess, L., Folkner, W.M., Durante, D., Parisi, M., Kaspi, Y., Galanti, E., Guillot, T., Hubbard, W.B., Stevenson, D.J., Anderson, J.D., Buccino, D.R., Gomez Casajus, L., Milani, A., Park, R.S., Racioppa, P., Serra, D., Tortora, P., Zannoni, M., Cao, H., Helled, R., Lunine, J.I., Miguel, Y., Militzer, B., Wahl, S., Connerney, J.E.P., Levin, S.M., & Bolton, S.J., (2018). Measurement of Jupiter's asymmetric gravity field. Nature 555. doi:10.1038/nature25776

Iess, L., Militzer, B., Kaspi, Y., Nicholson, P.D., Durante, D., Racioppa, P., Anabtawi, A., Galanti, E., Hubbard, W.B., Mariani, M.J., Tortora, P., Wahl, S., & Zannoni, M., (2019). Measurement and implications of Saturn's gravity field and ring mass. Science (80-.). 2965, eaat2965. doi:10.1126/science.aat2965

Jacobson, R. A., R. J. Haw, T. P. McElrath, & P. G. Antreasian. (1999) A comprehensive orbit reconstruction for the Galileo Prime Mission in the J2000 system. Presented at AAS/AIAA Astrodynamics Specialist Conference, American Astronautical Society, Girdwood, Alaska.

Jia, X., Kivelson, M. G., Khurana, K. K., & Kurth, W. S. (2018). Evidence of a plume on Europa from Galileo magnetic and plasma wave signatures. Nature Astronomy, 2(6), 459.

Kaspi, Y., Galanti, E., Hubbard, W. B., Stevenson, D. J., Bolton, S. J., Iess, L., ... & Durante, D. (2018). Jupiter's atmospheric jet streams extend thousands of kilometres deep. Nature, 555(7695), 223.

Kaula, W.M., (1963). Determination of the Earth's gravitational field. Rev. Geophys. doi:10.1029/RG001i004p00507

Kivelson, M. G., Khurana, K. K., Russell, C. T., Volwerk, M., Walker, R. J., & Zimmer, C. (2000). Galileo magnetometer measurements: A stronger case for a subsurface ocean at Europa. Science, 289(5483), 1340-1343.

Kliore, A. J., Hinson, D. P., Flasar, F. M., Nagy, A. F., & Cravens, T. E. (1997). The ionosphere of Europa from Galileo radio occultations. Science, 277(5324), 355-358.

Lainey, V. et al. (2020), New tidal paradigm in giant planets supported by rapid orbital expansion of Titan, Nature Astronomy (submitted).

Mariotti, G., & P. Tortora. (2013) "Experimental validation of a dual uplink multifrequency dispersive noise calibration scheme for Deep Space tracking." Radio Science 48.2: 111-117.

Matsuyama, I., Beuthe, M., Hay, H. C., Nimmo, F., & Kamata, S. (2018). Ocean tidal heating in icy satellites with solid shells. *Icarus*, *312*, 208-230.

Milani, Andrea, & Giovanni Gronchi. (2010) Theory of orbit determination. Cambridge University Press.

Modenini, D., & Tortora, P., (2014). Pioneer 10 and 11 orbit determination analysis shows no discrepancy with Newton-Einstein laws of gravity. Phys. Rev. D 90, 022004. doi:10.1103/PhysRevD.90.022004

© 2021. Licensed under the Creative Commons CC-BY-NC-ND 4.0
http://creativecommons.org/licenses/by-nc-nd/4.0/

Moore, W. B., & Schubert, G. (2000). The tidal response of Europa. Icarus, 147(1), 317-319.

Phillips, C. B., & Pappalardo, R. T. (2014). Europa clipper mission concept: exploring Jupiter's ocean moon. Eos, Transactions American Geophysical Union, 95(20), 165-167.

Phipps, P. H., Withers, P., Buccino, D. R., & Yang, Y. M. (2018). Distribution of Plasma in the Io Plasma Torus as Seen by Radio Occultation During Juno Perijove 1. Journal of Geophysical Research: Space Physics, 123(8), 6207-6222.

Roth, L., Saur, J., Retherford, K. D., Strobel, D. F., Feldman, P. D., McGrath, M. A., & Nimmo, F. (2014). Transient water vapor at Europa's south pole. Science, 343(6167), 171-174.

Serra, D., Lari, G., Tommei, G., Durante, D., Gomez Casajus, L., Notaro, V., ... & Bolton, S. J. (2019). A solution of Jupiter's gravitational field from Juno data with the orbit14 software. Monthly Notices of the Royal Astronomical Society, 490(1), 766-772.

Schubert, G., Anderson, J. D., Spohn, T., & McKinnon, W. B. (2004). Interior composition, structure and dynamics of the Galilean satellites. Jupiter: The planet, satellites and magnetosphere, 1, 281-306.

Sparks, W. B., Hand, K. P., McGrath, M. A., Bergeron, E., Cracraft, M., & Deustua, S. E. (2016). Probing for evidence of plumes on Europa with HST/STIS. The Astrophysical Journal, 829(2), 121.

Spencer, J. R., Tamppari, L. K., Martin, T. Z., Travis, L. D. (1999). Temperatures on Europa from Galileo Photopolarimeter-Radiometer: Nighttime Thermal Anomalies. Science 284, 1514.

Tortora, P., Zannoni, M., Hemingway, D., Nimmo, F., Jacobson, R. A., Iess, L., & Parisi, M. (2016). Rhea gravity field and interior modeling from Cassini data analysis. Icarus, 264, 264-273.

Tricarico, P. (2014), Multi-Layer Hydrostatic Equilibrium of Planets and Synchronous Moons: Theory and Application To Ceres and To Solar System Moons, Astrophys. J., 782(2), 99, doi:10.1088/0004-637X/782/2/99.

Zannoni, M., & Tortora, P., (2013). Numerical Error in Interplanetary Orbit Determination Software. J. Guid. Control. Dyn. 36, 1008–1018. doi:10.2514/1.59294

Zannoni, M., Tommei, G., Modenini, D., Tortora, P., Mackenzie, R., Scoubeau, M., Herfort, U., Carnelli, I., 2018. Radio science investigations with the Asteroid impact mission. Adv. Sp. Res. 62, 2273–2289. doi:10.1016/j.asr.2017.12.003

Zannoni, M., Hemingway, D., Gomez Casajus, L., & Tortora, P. (2020), The gravity field and interior structure of Dione, Icarus (in press). doi: 10.1016/j.icarus.2020.113713

Zimmer, C., Khurana, K. K., & Kivelson, M. G. (2000). Subsurface oceans on Europa and Callisto: Constraints from Galileo magnetometer observations. Icarus, 147(2), 329-347.

© 2021. Licensed under the Creative Commons CC-BY-NC-ND 4.0
http://creativecommons.org/licenses/by-nc-nd/4.0/